Original Research Paper

Thermodynamic Inference of the Antioxidant Process of Malic Acid and Its Structural Analogs

[1,2]Han Wu, [1]Wenhao Dong, [1]Yanhong Qiu and [1]Changbin Liu

[1]*School of Biological Engineering, Dalian Polytechnic University, Dalian, China*
[2]*Inner Mongolia Kunming Cigarette Limited Liability Company, Technical Research Center Biological Enzyme Development Laboratory, Hohhot, China*

Abstract: Two structural analogs of Malic Acid (MA), 2-isopropylmalic Acid (2-IPMA), and 3-isopropylmalic Acid (3-IPMA) were recently identified and separated from wine. Although they have been shown to have antioxidant activity, the mechanism of their actions is still unclear. Antioxidant activities of 2-IPMA and MA were tested through DPPH, ABTS, and PTIO methods and the antioxidant-related thermodynamic properties were evaluated using Density Functional Theory (DFT) to deduce their thermodynamic process and antioxidant mechanism. Results showed that all three organic acids had the potential to scavenge free radicals and 2-IPMA showed higher antioxidant activity. In addition, the C2-hydroxy groups of 2-IPMA and 3-IPMA showed the antioxidant activity. As the singlet state of most antioxidants is more stable than the triplet state, it was predicted that 2-IPMA and 3-IPMA would lose hydrogen through double Hydrogen Atom Transfer (HAT), Sequential double Proton Loss Double Electron Transfer (SPLET) and Double Electron Transfer Proton Transfer (dET-PT) methods in gas-phase to form 4-methyl-3-oxopentanoic acid and 3-methyl-2-formylbutyric acid, respectively. Based on the principle of minimum consumption first occurrence, the pathways of 2-IPMA and 3-IPMA to radical scavenging were in the following order: HAT, Bond Dissociation Energy (BDE), and SPLET. The results of the calculation confirmed the hypothesis of this study and suggested that the oxidation resistance of the two MA analogs favored the HAT process in terms of reaction enthalpy thermodynamics.

Keywords: 2-IPMA, 3-IPMA, Antioxidant Activity, DFT Calculations, HAT

Introduction

Free radicals are produced by metabolic processes, physiological activities, and the inhalation of external dust particles (Hussain *et al.,* 2003; Guo *et al.*, 2021 Ginter *et al.,* 2014). However, moderate concentrations of Reactive Oxygen Species (ROS) are beneficial (Aljerf and Aljerf, 2023). This is because they can quench exogenous microorganisms, and regulate cell division and stress response, which play a positively mediating role in normal physiological activities. When there is an excess of free radicals, the metabolic balance of protein, lipids, and DNA will be damaged which can lead to diseases such as diabetes, cardiovascular disease, and cancer among other diseases (Hussain *et al.,* 2003; Amic *et al.,* 2018; Halliwell *et al.,* 1992). There are many kinds of free radicals in biological systems, among which the oxygen-containing radicals are dominant, including superoxide anion ($O_2\bullet-$) conjugated acid hydroperoxy (HOO•), hydroxyl radical (HO•), alkoxy radical (RO•), peroxyl radical (ROO•), nitric oxide radical (NO•) and nitric oxide radical (NO$_2$•), among others. Furthermore, the human body can produce free radicals that have paired electrons, which are prone to loss. They include singlet oxygen ($1O_2$), hydrogen peroxide (H_2O_2), peroxynitrite (ONOO−), and hypochlorous acid (HOC$_1$) among others which are collectively referred to as ROS (Pier-Giorgio, 2000; Oliveira *et al.,* 2011; Aruoma *et al.,* 1998).

To maintain the balance, excess ROS are broken down by the metabolism of the body or by ingesting antioxidants (McCord *et al.,* 1969). Products derived from grapes have a wide range of antioxidant activities. For instance, grape pomace can promote animal oxidative stress (Junxing *et al.,* 2018; 2017). Many ingredients in grape seeds such as unsaturated fatty acids, polyphenols, vitamin E, and phytosterols are also reported to have antioxidant activity (Natacha *et al.,* 2015; Karaman *et al.,* 2015). Phenolic compounds have been identified as the main part of antioxidant in wine (Frankel *et al.,* 1993; Pace-Asciak *et al.,* 1995; Frankel *et al.,* 1995; Hayek *et al.,* 1997). However,

recent studies have shown that structural analogs of MA, 2-IPMA, and 3-IPMA have antioxidant activity (Pérez-Gálvez *et al.,* 2020; Rivera *et al.,* 2020; Massimo *et al.,* 2019) and the half-maximal Effective Concentration (EC50) values are 1/90 and 1/74 of anthocyanins, respectively (Rohan *et al.,* 2018).

There are two types of oxidation reactions in wine: Enzymatic oxidation and non-enzymatic oxidation. The main enzymes involved in the enzymatic oxidation include Superoxide Dismutase (SOD), Catalase (CAT), Glutathione S-Transferase (GST), selenium glutathione peroxidase (Se-GSH-Px), Thioredoxin Reductase (TrxR) and Aldosterone Reductase (AKR). The non-enzymatic oxidation parts in substances containing benzene rings are mostly due to the phenolic hydroxyl group, but a few are due to carboxyl, methoxy, and amino groups (Annia *et al.,* 2016; Oliveira *et al.,* 2011). Most antioxidant studies focus on phenols, flavonoids, and other substances with intense antioxidant activity, whereas the low molecular weight organic acids with weak antioxidant activity have attracted less attention (Yunus *et al.,* 2016).

Density Functional Theory (DFT) is a computational quantum mechanical method that revolutionized the field of electronic structure calculations by focusing on electron density rather than wave functions. DFT's Kohn-Sham approach transforms the complex many-body problem into a set of one-electron equations, providing an efficient way to predict molecular properties and reactivity. The accuracy of DFT hinges on the exchange-correlation function, which approximates the effects of electron interactions. While the exact form of this function is unknown, various approximations have been developed, each with its strengths and limitations. In antioxidant research, DFT plays a crucial role by enabling the detailed analysis of antioxidants' electronic structures, which is vital for understanding their redox properties and reactivity. It helps in calculating molecular orbitals, particularly the HOMO and LUMO, which are key to assessing the antioxidant capacity. DFT also aids in exploring reaction mechanisms and predicting the thermodynamics and kinetics of antioxidant actions, such as hydrogen atom transfer and electron transfer processes. Despite challenges with certain systems, DFT's versatility and cost-effectiveness make it an indispensable tool for studying the complex interactions of antioxidants with reactive oxygen species, thereby supporting the design of more effective antioxidant compounds and deepening our understanding of oxidative stress mechanisms (Erik and Vladimír, 2006; Borges *et al.,* 2016; Zhongping *et al.,* 2014). Although 3-IPMA and 2-IPMA have been shown to have antioxidant activity, the mechanism of their actions remains unclear (Frankel *et al.,*1995).

Furthermore, there are few theoretical studies on the antioxidants of low molecular weight organic acids. Therefore, the current study, verified the antioxidant activity of 2-IPMA using DPPH•, ABTS•+, and PTIO•, as well as deduced the thermodynamic process and antioxidant mechanism by conformational and thermodynamic calculations.

Materials and Methods

Determination of Antioxidant Activity

2-IPMA (98%, Sigma-Aldrich) was obtained from Merck. DPPH (96%), ABTS (98%), and PTIO (98%) were purchased from Macklin (Shanghai Macklin Biochemical Co., ltd), MA (99%) was purchased from Shanghai Dingfen Chemical Technology Co., ltd., KH_2PO_4 (Chengdu chemical reagent factory) were bought through sangon biotech co., ltd.

Determination of Antioxidant Activity by DPPH

The DPPH (2-2-Diphenyl-1-Picrylhydrazyl) method is a widely used assay in chemistry and biochemistry for determining the antioxidant capacity of substances. DPPH is a stable free radical with a purple color. It has an unpaired electron, which gives it its characteristic color. When antioxidants are added to a DPPH solution, the antioxidants donate an electron to the DPPH radical, neutralizing it and forming a stable, non-radical compound. The decrease in absorbance at a specific wavelength (usually around 517 nm) is measured using a spectrophotometer. This absorbance is directly related to the number of electrons accepted, indicating the antioxidant capacity. However, like any other analytical method, DPPH has its limitations, such as only measuring the ability of a substance to donate an electron, being sensitive to reaction conditions, being limited to hydrophilic antioxidants, being conducted *in vitro* under controlled conditions, etc. Despite these limitations, the DPPH assay remains a popular and relatively simple method for estimating the antioxidant capacity of substances.

Preparation of sample solution: 6.25 mg of 2-IPMA solid powder dissolved in 50 mL absolute ethyl alcohol. The absorbed 0.5, 1-3 mL were separately diluted to 50 mL using absolute ethyl alcohol. Aliquots of 0.5, 1-3 mL were separately diluted to 50 mL using absolute ethyl alcohol. Solutions of 2-IPMA at concentrations of 1.25, 2.5, and 5-7.5 mg/L were prepared, respectively, and designated as A1, A2, A3, and A4 to assess the antioxidant activity at varying concentrations. According to the EC50 previously reported (Amic *et al.,* 2018), 4.8 g/L of the 2-IPMA solution was prepared as A5 and a similar amount of MA was also prepared as A6.

Preparation of DPPH stock solution: 0.0710 g of DPPH solid powder was accurately weighed and

dissolved in absolute ethyl alcohol and diluted to 100 mL to prepare the stock solution (1.80 mmoL/L). This was then refrigerated in a brown bottle protected from light.

Preparation of DPPH working solution: 5 mL of DPPH stock solution was accurately transferred and diluted to 50 mL with absolute ethyl alcohol to prepare 0.180 mm/L DPPH working solution and prepare the working solution on the spot.

The corresponding reagents were added and placed in a dark place to react 30 min at 25℃ (as shown in Table S1). The absorbance was measured using the UV spectrophotometer at 517 nm. The radical scavenging rate was calculated using Eq. (1). Three parallel experiments were conducted and the data presented are the average of these three measurements:

Free radical scavenging efficiency

$$(\%) = \frac{A_{con} - (A_{sam} - A_{bla})}{A_{con}} \times 100\% \tag{1}$$

where, A_{con}, A_{sam}, and A_{bla} are the absorbance of the control group, sample group, and blank group respectively.

Determination of Antioxidant Activity by ABTS•+

Preparation of Sample Solution: Samples 7 (4800 mg/L) and 8 (3654 mg/L) were prepared using deionized water instead of absolute ethyl alcohol following the same method as for samples A5-6.

96 mg ABTS•+ power was dissolved in deionized water and diluted to 25 mL to prepare the ABTS•+ stock solution and 16.6 mg $K_2SO_2O_8$ was dissolved in absolute ethyl alcohol and diluted to 25 to prepare the $K_2SO_2O_8$ buffer (2.45 mmol/L) according to previously reported procedures (Stéphanie *et al.,* 2009; Re *et al.,* 1999; Wootton-Beard *et al.,* 2011). The mother solution and buffer (2:1, v/v) were mixed and kept in the dark for between 12-16 h to form stable ABTS•+ radicals. They were then refrigerated in a brown bottle protected from light.

Preparation of ABTS•+ working solution: 200 mL of ABTS•+ stock solution was diluted with deionized water to form 5000 mL. Corresponding reagents were added, and placed in a dark place for the reaction at 25℃ to occur and absorbance of the UV spectrophotometer was recorded at 734 nm (as shown in Table S2).

Table S1: Experimental group for determination of antioxidant activity by DPPH• (mL)

	DPPH•	Simple	Absolute ethyl alcohol
A_{con}	2.8		0.7
A_{bla}		0.7	2.8
A_{sam}	1.8	0.7	

Table S2: Experimental group for determination of antioxidant activity by ABTS•+ (mL)

	ABTS•+	Simple	Deionized water
A_{con}	2.8		0.7
A_{bla}		0.7	2.8
A_{sam}	1.8	0.7	

Table S3: Experimental group for determination of antioxidant activity by PTIO• (mL)

	PTIO•	Simple
A_{con1}	3.5	
A_{sam}	1.8	0.7

Determination of Antioxidant Activity by PTIO

A PBS solution was prepared by adding 1.36 g of KH_2PO_4 and 0.316 g of NaOH into 200 mL of deionized water, resulting in a solution with a pH of 7.4, which was then stored in the refrigerator.

Preparation of PTIO solution storage solution: 0.025 g of PTIO powder was dissolved in PBS solution and diluted to 50 mL to form the storage solution (2.144 mmol/L) and then refrigerated at 4℃ in a brown bottle away from light.

Preparation of PTIO working solution: The PTIO working solution was made by mixing 10 mL of PTIO stock solution and 30 mL of PBS solution.

The corresponding reagents were added and the mixture was placed in a dark place to react at 25℃. The absorbance was then recorded using the UV spectrophotometer at 557 nm (Table S3). The radical scavenging rate was calculated according to Eq. (2) shown below:

Free radical scavenging efficiency

$$(\%) = \frac{A_{con1} - A_{sam}}{A_{con1}} 100\% \tag{2}$$

where, A_{con1} and Asam are the absorbances of the pure PTIO control group and sample group respectively.

Calculation Using Density Functional Theory (DFT)

The calculations were performed using Gaussian 16 program package, B3LYP functional, and TZVP basis groups (Frisch *et al.*, 2016; Becke, 1993; Chengteh *et al.*, 1988; Burkhard *et al.*, 1989; Ansgar *et al.*, 1992; 1994). The geometries of malic acid and its derived species, including hydroxyl radicals, various ions, and electron states, were optimized using the B3LYP functional in conjunction with the TZVP basis set. This approach involved a comprehensive optimization of molecular geometries to ascertain the most stable conformations, followed by frequency calculations to confirm that these structures represent energy minima on the

potential energy surface, characterized by the absence of imaginary frequencies. Further, the calculations in the study were performed in the gas phase using ethyl alcohol and pentyl ethanoate as the implicit solvent model. These models are selected to encapsulate the micro environmental influences on molecular behavior, with ethanol representing a polar solvent and pentyl ethanoate simulating a lipid-like environment. For open-shell systems, which are characterized by the presence of unpaired electrons, we have adopted unrestricted calculations. This approach allows for the independent optimization of the wave function for alpha and beta electrons, thereby accurately reflecting the electronic structure of radicals and other species with open-shell configurations. The use of unrestricted calculations ensures that the spatial and spin orientations of the unpaired electrons are properly accounted for, leading to a more precise depiction of the system's ground state and its reactivity. In our computations, we have meticulously set up the molecular geometries and performed geometry optimizations to identify the most stable conformations. Subsequent frequency calculations have been executed to verify that these optimized structures correspond to energy minima, as indicated by the absence of imaginary frequencies. The results found that there was no spin contamination of the free radical species.

We employed the Multiwfn software to conduct an in-depth analysis of molecular geometric structure parameters. Multiwfn is a versatile tool that allows for the extraction and visualization of a wide array of molecular properties directly from quantum chemical packages (Lu and Chen, 2012; Lu *et al.*, 2015; Tian and Fei-Wu, 2011). Utilizing this software, we have calculated key structural parameters such as bond lengths, bond angles, and dihedral angles. Furthermore, Multiwfn facilitated the analysis of the Highest Occupied Molecular Orbital (HOMO) and Lowest Unoccupied Molecular Orbital (LUMO) energy levels. These orbitals are pivotal in determining the molecular reactivity and the electron distribution within the molecules. The energy gap between HOMO and LUMO is a significant indicator of the molecule's susceptibility to chemical reactions and its potential as an antioxidant. To visualize the molecular surface electrostatic potential, we turned to the Visual Molecular Dynamics (VMD) software. With VMD, we were able to render the molecular surfaces and calculate the electrostatic potentials. Additionally, we used Multiwfn to compute THE hydroxyl bond dissociation enthalpy, a critical parameter for evaluating the antioxidant capacity of molecules. This computation involves determining the energy required to break the hydroxyl bond, which is directly related to the molecule's ability to donate hydrogen atoms and neutralize free radicals.

In addition, VMD was used to create the images while the enthalpy and free energy were calculated at 298.15 K using the thermodynamic data for free radicals, protons, and electrons in HAT, Sequential Electron-Proton Transfer (SET-PT) and SPLET (Humphrey *et al.*, 1996). In our computational study, we meticulously selected and applied thermodynamic data to calculate the enthalpy (ΔH) and free energy (ΔG) for the reactive species at the standard temperature of 298.15 K. This temperature is commonly used as it approximates room temperature and is a standard reference point in thermodynamics. For the HAT process, where a hydrogen atom is transferred from a donor molecule to an acceptor, we considered the enthalpy and free energy changes associated with the formation of the free radicals and the breaking of the hydrogen-donating bond. In the SET-PT mechanism, which involves the sequential transfer of a proton and an electron, we utilized the relevant thermodynamic data to calculate the energy changes for each step. This includes the dissociation of the proton and the subsequent electron transfer, for which we accounted for the solvation effects and the energy levels of the species involved. For the SPLET process, where a single proton and electron are transferred simultaneously, we applied the appropriate thermodynamic data to estimate the energy required for this concerted mechanism. This included calculations of the enthalpy and free energy for the formation of the resulting radicals and the dissociation of the proton-electron pair. Throughout our calculations, we ensured that the thermodynamic data were compatible with the computational methods and basis sets employed and we considered the solvent environment and any potential interactions that could affect the enthalpy and free energy changes.

Results and Discussion

Free Radical Scavenging Activities of 2-IPMA and MA

The DPPH•, ABTS•+, and PTIO• are free radicals commonly used in antioxidant experiments (Stéphanie *et al.*, 2009; Xican, 2018-2017; Xilan *et al.*, 2013; Jiang *et al.*, 2020). Their discrepancies are shown in Table (1). DPPH• and ABTS•+ are usually used as indicators to evaluate the radical scavenging capacity *in vitro*. The active sites of these free radicals are all on a single Nitrogen (N) atom in the molecule (Eklund *et al.*, 2005). Unlike DPPH•, the free radical part of ABTS•+ was an N ion with a single charge. The N atom at the center of DPPH• contains a single electron due to the particularity of its molecular structure and it has a strong absorption peak at 520 nm. Further, DPPH• prefers to react with small molecular antioxidants because of the

steric effect (Blois, 1958; Brand-Williams *et al.*, 1995). The DPPH• reagent in ethanol solution is dark purple, whereas the ABTS•+ solution was dark green. When antioxidants were added to DPPH•, they provide protons or electrons to inactivate the free radicals, reducing the 520nm peak and turning the solution color to pale yellow or colorless (Shimada *et al.*, 1992; Kumaran and Joel Karunakaran, 2006). However, PTIO• has the advantage of outstanding stability and is easily affected by the environment. According to research conducted by Li Xican, it was reported that DPPH• and ABTS•+ should not be used for most of the phenolic hydroxyl groups (Stéphanie *et al.*, 2009). Further, PTIO• can simulate the radical quenching process of oxygen-containing radicals, as compared to the first two nitrogen-containing radicals. It was found that when enough antioxidants were added, PTIO•, which is violet-blue, fades and the UV absorption peak at 734 nm decreases.
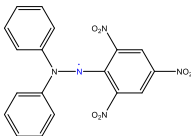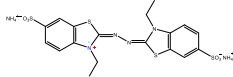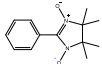
In the present study, it was found that the radical scavenging efficiency of 2-IPMA at low concentrations was poor. The maximum radical scavenging rate of samples A1-A6 was 4.4%, after a reaction time of 90 min (Fig. 1, S1-4). Further, it was noted that when the concentration was up to the EC50 (A5, 2.72×10^4 mmol/L), the change from dark purple (DPPH•) to pale yellow

(DPPH) could be clearly observed. The absorbance of the sample solution at 520nm was also significantly reduced, while the free radical scavenging ability was significantly enhanced (Fig. 1, S5). The radical scavenging rate reached 23% at 30 min and then slowly increased. The radical scavenging rate reached 26% after 180 min however, the ability of MA to scavenge free radicals (Fig. 1, S6) was only half of that 2-IPMA.

Results of ABTS•+ radical scavenging by 2-IPMA are shown in Fig. (1, S7. Within 20 min, the rate of radical scavenging potential for 2-IPMA sharply rose to 40%, whereas the radical scavenging rate of MA peaked at 3.8% within 10 min (Fig. 1, S8). Different from DPPH•, ABTS• + prefers the ET pathway to achieve stability, which leads us to believe that 2-IPMA is more susceptible to electron loss than MA.

The 2-IPMA and MA showed distinct free radical scavenging activities in two pH solutions of PTIO•. Further, the 2-IPMA had 19.0-20.0% radical scavenging rate at pH 7.4-4.5, while MA had 16.0-16.8% radical scavenging rate at pH 7.4-4.5 (Fig. 1). Moreover, it was noted that there was little discrepancy in pH, the scavenging rate was slightly higher at pH the scavenging efficiency of PTIO• between two different pH, the scavenging rate was slightly higher at pH 4.5.

Table 1: Similarities and differences of three antioxidant reagents

|	*DPPH·*	*ABTS·+*	*PTIO·*
Constitutional formula			
Molecular weight	394.32	548.68	233.29
the active site of free radical	—N·	—N·+	—O
Electrified condition	neutral radical	cationic radical	neutral radical
Solubility	absolute ethyl alcohol	de-ionized water	de-ionized water
Experimental color change	purple → pale yellow/colorless	dark green → colorless	bluish violet→ colorless
Detection wavelength	519 nm	734nm	557nm
Radical scavenging principle	*HAT*	*ET*	*ET+PT*
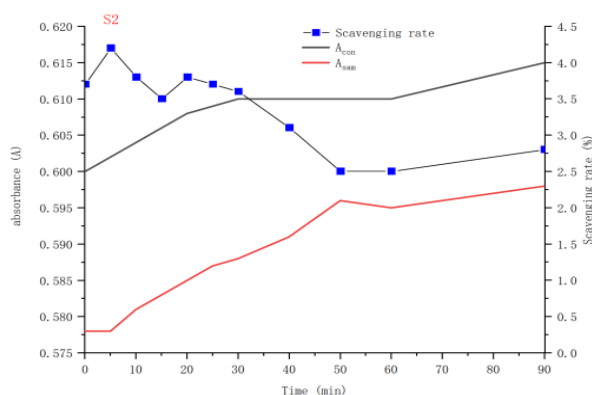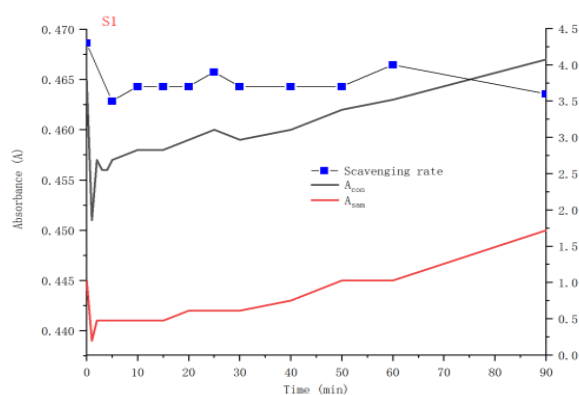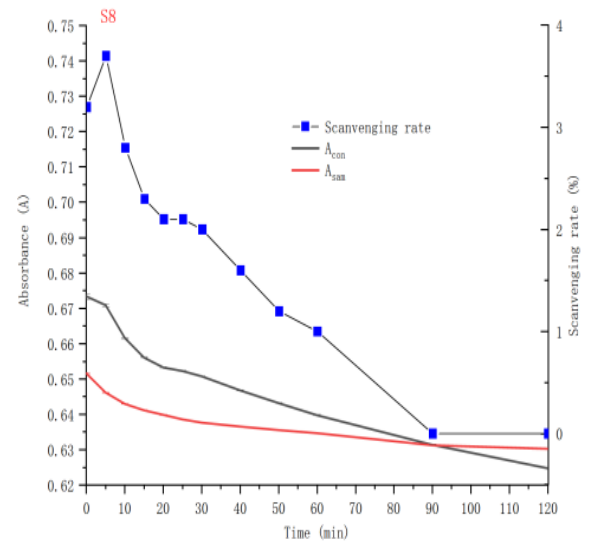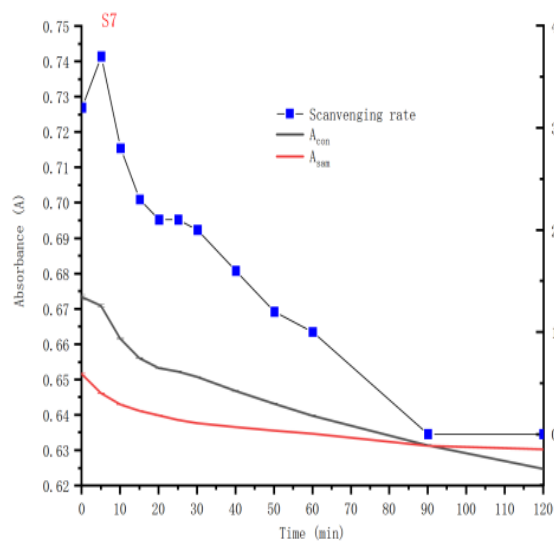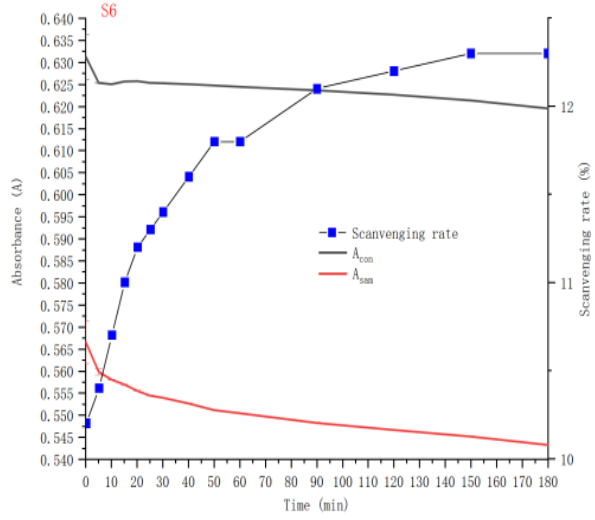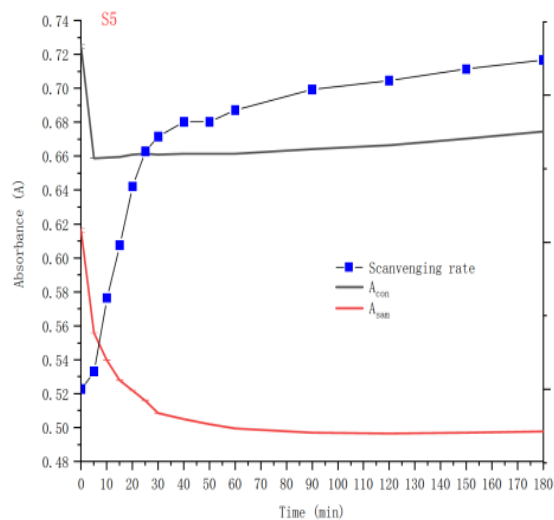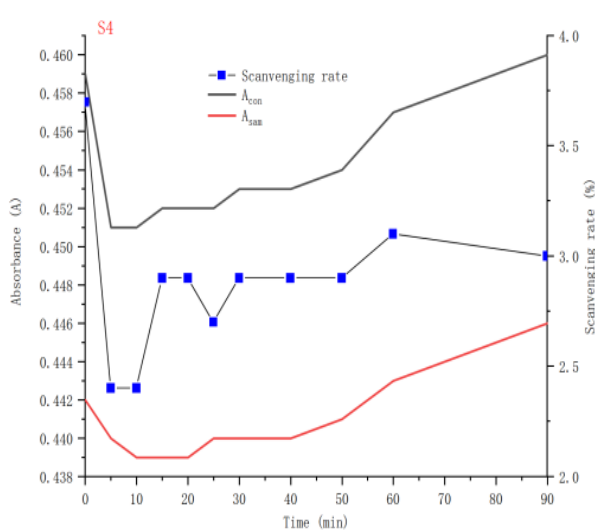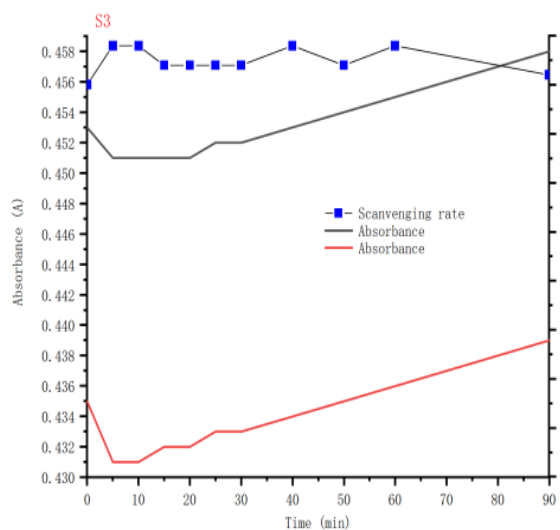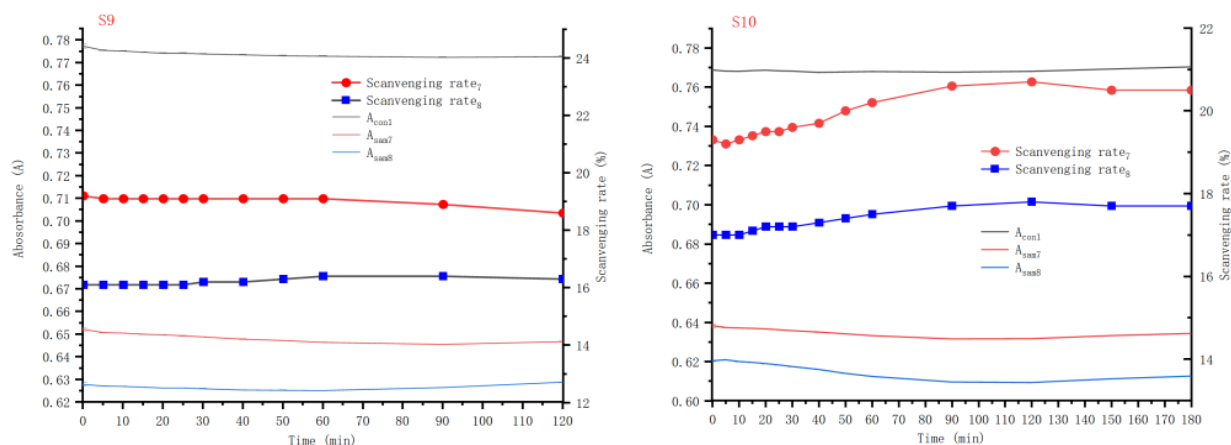
Fig. 1: Radical scavenging curves of 2-IPMA and MA. S1–S6 represent the DPPH˙ radical scavenging curves of Samples A1-6 respectively; S7-8 represent the ABTS˙⁺ radical scavenging curves of Samples A7-8 respectively; S9-10 represent the PTIO˙ radical scavenging curves of A7 (pH = 7.4) and A8(pH = 4.5) respectively. The experimental results are expressed as the mean standard deviation, n = 3

Molecular Structure and *Conformation Analysis*

A previous study conducted by Bin *et al.* (2021) reported that the free radical scavenging activity of certain groups could be predicted by reaction sites in molecules. Molecular structure, also known as molecular plane structure, molecular shape, or molecular geometry, is used to describe the three-dimensional arrangement of atoms in a molecule based on spectroscopic data (Qiu *et al.*, 2017). However, the bond angle and dihedral angle have little effect because MA, 2-3-IPMA did not have conjugated structures. The optimal structures of the three kinds of molecules with all the atoms labeled were as shown in Fig. (2) whereas the parameters of each bond length in the molecule were s shown in Table (2). The molecular structures of three kinds of MA were optimized by the B3LYP/TZVP method Fig. (3). In addition, the main structural parameters were as shown in Table (2).

Data analysis shows that the length of the C-C bond in 2-IPMA ranged from 0.151~0.154 nm, and those of 3-IPMA and MA ranged from 0.152~0.153 nm and 0.151~0.153 nm, respectively. Therefore, they are all in the length range of stable C-C bond (0.154 nm) with little discrepancy (Qiu *et al.*, 2017).
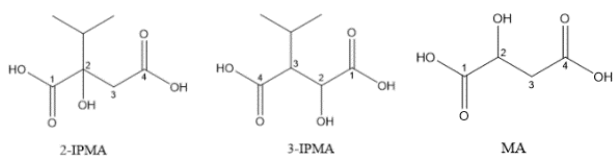

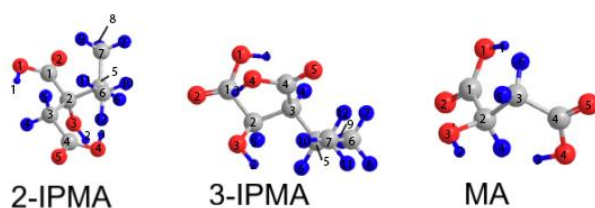**Fig. 2:** Molecular structure of 2-IPMA,3-IPMA and MA

Fig. 3: Molecular optimized configurations of 2-IPMA,3-IPMA, and MA Gray: C atom; Red: O atom; Blue: H atom

Table 2: Main bond parameters of 2-IPMA and 3-IPMA (bond length: Å)

Bond	2-IPMA	3-IPMA	MA
O_1—H_1	0.970	0.971	0.970
O_3—H_2	0.965	0.964	0.969
O_4—H_3	0.970	0.970	0.971
C_1—O_1	1.353	1.357	1.344
C_2—O_3	1.414	1.431	1.409
C_4—O_4	1.361	1.359	0.971
C_1—C_2	1.539	1.528	1.518
C_2—C_3	1.577	1.529	1.530
C_3—C_4	1.510	1.517	1.511

According to the molecular valence bond theory, the strength of the bond in the molecule is inversely proportional to its length (Sason *et al.*, 2021; Dunning *et al.*, 2021) Further, the C_2-C_3 bonds have the highest value in all the C-C bonds of the three kinds of molecules whereas C_2-O_3 bonds have the highest value in all C-O bonds. However, the O_3-H_2 bonds have the smallest value in all O-H bonds and the bond lengths of the same bonds had little discrepancy.

Since the bond lengths of the O-H bond in the carboxyl group and the O-H bond in the alcohol hydroxyl group are very similar, it suggests that the antioxidant activities of 2-3-IPMA depend on the difficulty of H transfer from these groups to the free radical and the stability of the resulting free radical after hydrogen transfer.

Frontier Orbital and *Orbital Energy Level Analysis*

HOMO contains higher energy among the molecular orbital energies, with electrons in this orbit being unstable and prone to leaving the orbit to provide electrons. In contrast, LUMO contains relatively low energy, with electrons in this orbit being stable and even capable of attracting high-energy electrons (Damian *et al.*, 2010). The energy difference, denoted as $\triangle E$ (LUMO-HOMO), reflects the energy required for the electronic transitions. The smaller the $\triangle E$, the less energy is required for electronic transitions, making the electrons easier to excite. Consequently, the molecule's reaction activity is stronger and the reaction is more likely to occur.

At the B3LYP/TZYP calculation level, the values of E_{LUMO}, E_{HOMO}, $\triangle E$(LUMO-HOMO) of 2-IPMA, 3-IPMA, and MA are as shown in Table (3). It is found that the E_{HOMO} values of 2-3-IPMA, and MA are -0.2818, -0.2829, and -0.2980, respectively, whereas the E_{LUMO} values are -0.0321, -0.0309 and -0.0340, respectively. It is also noted that the 3-IPMA is more likely to lose electrons than 2-IPMA and MA because the energy difference $\triangle E$ (LUMO-HOMO) for 3-IPMA was smaller than that for 2-IPMA and MA.

Molecular Orbital Contribution

The molecular orbitals (HOMO and LUMO) of the three kinds of MA are plotted using Multiwfn and VMD software (as shown in Fig. (4). The molecular orbital diagram enables the intuitive and qualitative analysis of the distribution of active sites within molecules that participate in reactions. The higher the electron cloud density of the HOMO, the more likely the molecule is to react with radicals. Moreover, areas with higher density may be the active sites for antioxidant reactions. The contributions of the hydroxyl groups in the three molecules to the molecular orbitals were calculated using the Multiwfn software Table (4).

Table 3: HOMO energy level, LUMO energy level, and energy level differences of 2-IPMA,3-IPMA, and MA (A.U.)

	2-IPMA	3-IPMA	MA
E_{LUMO}	-0.0321	-0.0309	-0.0340
E_{HOMO}	-0.2818	-0.2829	-0.2980
$\triangle E_{(LUMO-HOMO)}$	0.2497	0.2520	0.2640

Table 4: Proportions of hydroxyl groups of 2-3-IPMA, and MA to frontier molecular orbitals (%)

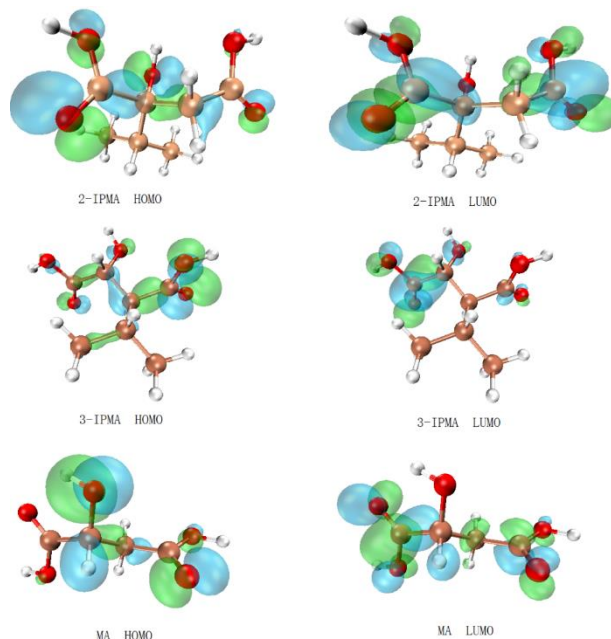|		2-IPMA	3-IPMA	MA
HOMO	O_1—H_1	5.853	1.584	0.862
	O_3—H_2	29.832	2.870	61.524
	O_4—H_3	0.759	8.328	2.377
LUMO	O_1—H_1	4.785	6.749	6.248
	O_3—H_2		5.372	0.091
	O_4—H_3	3.955	0.453	1.926

Fig. 4: The molecular orbital diagram of 2-IPMA,3-IPMA, and MA

From the molecular orbital diagram Fig. (4) and the proportion of hydroxyl groups in the three molecules occupying the molecular orbital Table (4), it is found that 2-IPMA has a larger proportion at the O_3-H_2 site, while 3-IPMA has a larger proportion at the O_4-H_3 site. Therefore, the antioxidant reactions probably occur over the molecular orbit.

Surface Electrostatic Potential (ESP) Analysis

Electrostatic potential refers to the work done to move the unit positive charge from an infinite distance to a point in and around the molecule. The molecular surface electrostatic potential is a significant parameter for studying noncovalent interactions. The part with high potential represents a nucleophilic reaction site and the opposite is an electrophilic reaction site. A previous study conducted by Bin *et al.* explained that the electroactive sites of 3-tert-Butyl-4-Hydroxyanisole (BHA) are distributed according to the electrostatic potential, with the oxygen atom having the lowest potential (Bin *et al.*, 2021).

Isosurface analysis with an electron density of 0.001 a u is performed in the study on the three molecules using Multiwfn and VMD software. The calculated results are shown in Fig. (5) and the electrostatic potential extremes of hydroxyl and carboxyl groups are shown in Table (5). In the surface electrostatic potential diagram, the yellow and blue balls referred to the electrostatic potential maximum point and the electrostatic potential minimum point, respectively. The distribution of the minimum point consistency of the three molecules is near the hydroxyl group of C_2 and the absolute value is obviously larger than

the carboxyl part. Therefore, the hydroxyl oxygen in the three molecules is easily attacked by the electrophilic group.

O-H BDE Analysis

BDE is the energy required to break or form a molecular bond which simultaneously represents a physical quantity of the bond's strength. It is evident that the larger the BDE, the more stable the bond is. On the contrary, the lower the BDE, the more reactive the bond. BDE is an important indicator of a molecule's capacity to scavenge free radicals.

The 2-3-IPMA can scavenge external free radicals through hydrogen extraction reactions. The low BDE indicates that the hydroxyl group has a higher rate of hydrogen abstraction. Therefore, it is suggested that the carboxyl and hydroxyl groups in each molecule of the three kinds of MA were involved in HAT. BDE can be calculated using Eq. (3):

$$BDE = Hr + Hh - HI \tag{3}$$

where, Hr is the enthalpy of the antioxidant radical after dehydrogenation, Hh is the enthalpy of the hydrogen radical and HI is the enthalpy of the antioxidant molecule.

Therefore, it is hypothesized that the spin multiplicities after each HAT are 2-4, respectively. Triple BDE of the three kinds of MA in gas-phase are shown in Table (6). It was found that the BDE of the three hydrogen atoms of 2-IPMA and 3-IPMA were both lower than those of the corresponding hydrogen atoms in the MA. Furthermore, after reaching a steady state at the first HAT, the BDE at other active sites also increased during the subsequent HAT. However, the third BDE value (104.692 kcal/moL) of MA was lower than the previous value in our calculations. Even though the energy required for the third HAT in MA, the total BDE (BDET, 315.029 kcal/moL) for MA was higher than that of 2-IPMA (301.256 kcal/moL) and 3-IPMA (310.916 kcal/moL). Therefore, it is inferred that 2-PIMA and 3-IPMA have stronger radical scavenging abilities.

Radical Scavenging Pathway Analysis

The Double HAT Mechanism

General theoretical reports on the radical scavenging potential of antioxidants are based on the single HAT (1H+/1e-) mechanism at the active site. In the study, the BDE values of each antioxidant site were calculated to represent the capacity for antioxidant activity.

According to the BDEs shown in Table (6), both 2-IPMA and 3-IPMA preferentially dissociate from C_2 in the gas phase. Further, the BDE values of C_2 in the 2-3-IPMA at distinct states, as shown in Table (7), differ in ethanol and pentyl ethanoate. When C_1 is in an anionic state, C_2 is more easily dissociated from the 2-IPMA in pentyl ethanoate. However, in ethanol, the 2-IPMA in a nonionic state is more likely to cause dissociation of C_2. When the solvent is ethanol or pentyl ethanoate, the C_1 and C_4 of 3-IPMA are both anionic and the C_2 is the most likely to break. In addition, the 3-IPMA in pentyl ethanoate is more easily broken than in ethanol. Furthermore, the BDE of C_2 in 3-IPMA was lower than that of 2-IPMA at the same conditions.

Table 5: Electrostatic potential maxima of 2-3-IPMA, and MA (kcal/mol)

	2-IPMA	3-IPMA	MA
H_1	53.679	53.381	58.354
H_2	35.535	46.358	27.463
H_4	51.016	45.877	48.918
O_1		-8.816	-8.854
O_2	-24.242	-32.343	-34.249
O_4	-10.061	-13.466	-16.649

Table 6: Hydroxyl dissociation enthalpies of 2-3-IPMA, and MA (kcal/mol)

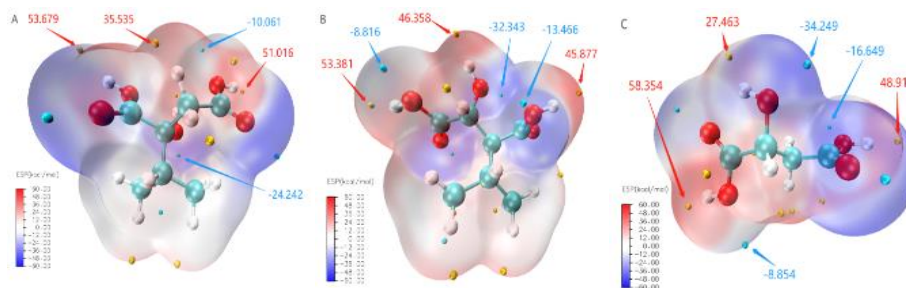| BDE		2-IPMA	3-IPMA	MA
BDE_1	H_1	93.422	102.167	106.473
	H_2	92.635	100.768	104.805
	H_4	94.297	103.284	104.724
BDE_2	H_1	103.502	105.615	107.262
	H_2			105.613
	H_4	104.380	104.092	
BDE_3	H_1		106.056	104.692
	H_2			
	H_4	105.119		
BDE_T		301.256	310.916	315.029

Fig. 5: The surface electrostatic potentials of 2-3-IPMA and MA. A: 2-IPMA; B: 3-IPMA; C:MA

Table 7: BDE values in different states of 2-3-IPMA, BDE_E = Ethanol, BDE_P = Pentyl ethanoate. (kcal/mol)

	$-C_1OOH \setminus -C_4OOH$		$-C_1OO^- \setminus -C_4OOH$		$-C_1OOH \setminus -C_4OO^-$		$-C_1OO^- \setminus -C_4OO^-$	
	BDE_E	BDE_P	BDE_E	BDE_P	BDE_E	BDE_P	BDE_E	BDE_P
2-IPMA	101.912	101.789	102.163	100.419	104.683	106.825	107.355	107.035
3-IPMA	101.947	101.529	101.463	98.629	99.398	106.166	94.856	93.284

The double HAT mechanisms of 2-3-IPMA were calculated in Figs. (6-7) and shown that they can scavenge radicals in non-polar media. The BDE1 of 2-IPMA and 3-IPMA indicates that the easiest extractable H atom is from the OH group on C_2, whereas the hardest extractable H atom is from the $-C_4OOH$ and $-C_1OOH$ groups of 2-IPMA and 3-IPMA, respectively.

It is worth noting that the energy cost of the second hydrogen atom extraction is greatly reduced. However, after the HAT reaction with the first free radical, the free radical becomes stable. Conversely, the antioxidant, after losing H, becomes active but is relatively stable towards free radicals, leading the antioxidants to change the structure of their active sites to achieve a steady state. For instance, the phenol molecule will become quinone after losing H. In addition, the phenoxy group may form a ring with other active sites that lose H to achieve a stable state. The formation of quinones or rings changes the multiplicity state to a singlet state. Further, after scavenging the free radicals, the structure of antioxidants changes, and new free radicals are formed. However, the activity of the new free radicals is much lower than that of the scavenged radicals. The antioxidants whose structure is also changed, form a stable product (Markovic *et al.*, 2016) The structures, stability, and spin multiplicity of 2-3-IPMA will also change after losing H.
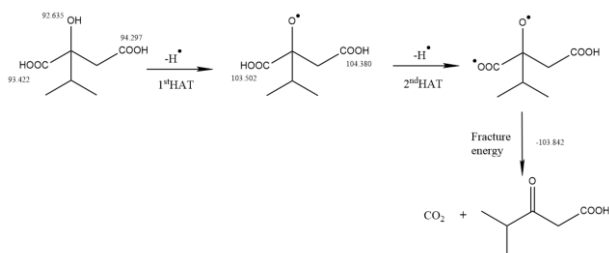

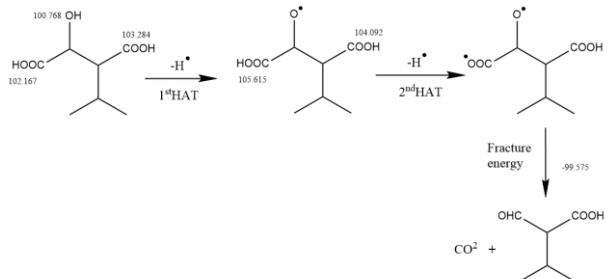**Fig. 6:** HAT pathway of 2-IPMA in gas-phase (kcal/mol)

Fig. 7: HAT pathway of 3-IPMA in gas-phase. (kcal/mol)

The variation trend of the total system energy shows that total system energy increases after each H is lost, making the system more unstable with each loss. After losing two consecutive H, the energy difference between the triplet and singlet states, known as the Fracture Energy (FE) is calculated to be 103.842 kcal/mol for 2-IPMA and 99.575 kcal/moL for 3-IPMA, respectively. As expected, the total energy of the singlet state in both polar and nonpolar solvents is always lower than that of the triplet state. Because of the absence of unpaired electrons in the structure, the final product obtained by breaking the C_1-C_2 band is 4-methyl-3-oxopentanoic acid and 3-methyl-2-formylbutyric acid, respectively. Moreover, the stable singlet state is more conducive to the occurrence of double HAT mechanism, which agrees with the report by Anouar *et al.* (2009)

The SPLET Mechanism

Considering the feasibility of the SPLET pathway in polar electrolytes, the enthalpies were calculated for the ionic and free radical states of 2-3-IPMA in the gas phase. It was evident that both 2-3-IPMA can undergo radical scavenging through the C_2-OH and -the C_1OOH. The thermodynamic data was characterized by Proton Affinity (PA) and Electron Transfer Enthalpy (ETE). The results of the current study are summarized in Figs. (8-9) and the electron, ion, and radical enthalpies used in this mechanism are presented in Table (S4).

In 2-IPMA, C_1 has a lower value of PA (315.543 kcal/moL) than C_2 (347.856 kcal/moL) and C4 (334.821 kcal/moL). According to the report of a previous study conducted by Ana Amić, the first step of the SPLET pathway is the deprotonation of the C_1 carboxyl group (Amic *et al.*, 2017; 2018). The second step is divided into two directions. One is the formation of a single free radical (bottom left, ETE = 93.867 kcal/moL) as the target. Then format a triplet state through the second PA2 (324.870 kcal/moL) and ETE2 (93.832 kcal/moL). Lastly, it costs 103.842 kcal/moL energy to form 4-methyl-3- oxovaleric acid. Consequently, the total energy cost of this process was 724.27 kcal/moL (Sa = PA1+ ETE1+ PA2+ ETE2+ FE).

The other direction in the second step of the SPLET pathway is to form the dianion through second proton transfers (top right, PA2 = 528.012 kcal/moL). In addition, 4-methyl-3oxopentanoic acid was then generated by changing the molecular structure after two consecutive electron transfers forming a triplet state. The total energy cost is similar to that in the first direction, 724.27 kcal/moL.

Table S4: Gas-phase enthalpies of H^+ and e^- (kcal/mol)

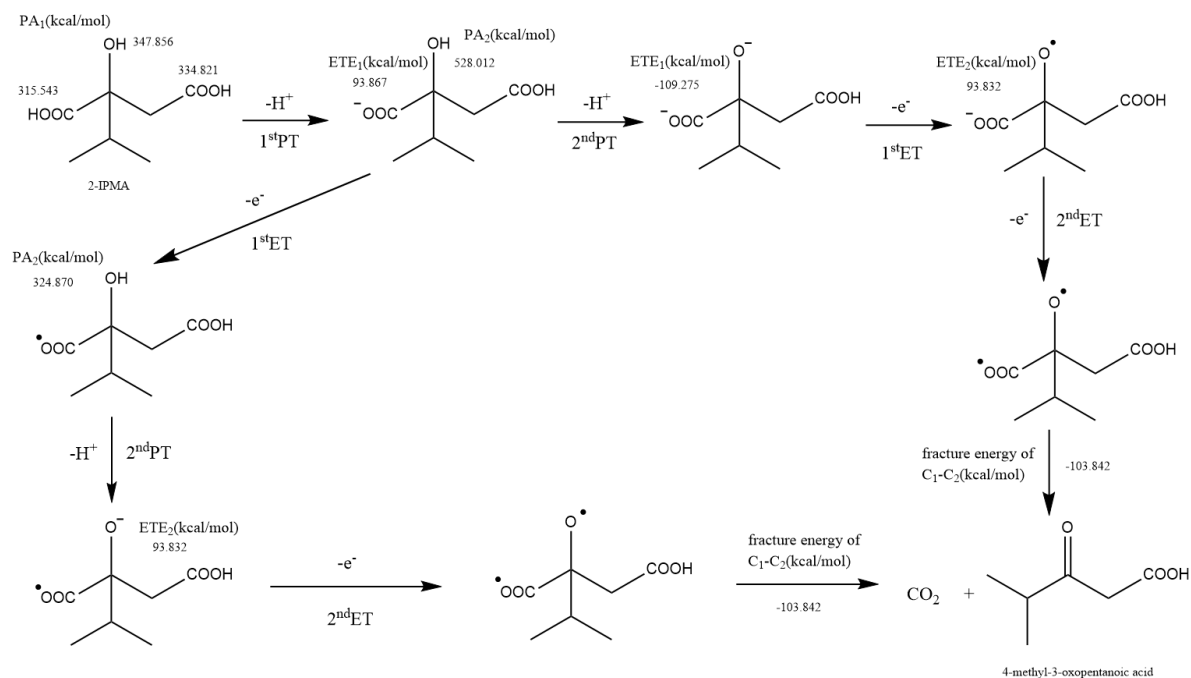| H ($H^{\cdot}$)	H (H^+)	H (e^-)
-313.755	1.481	0.752

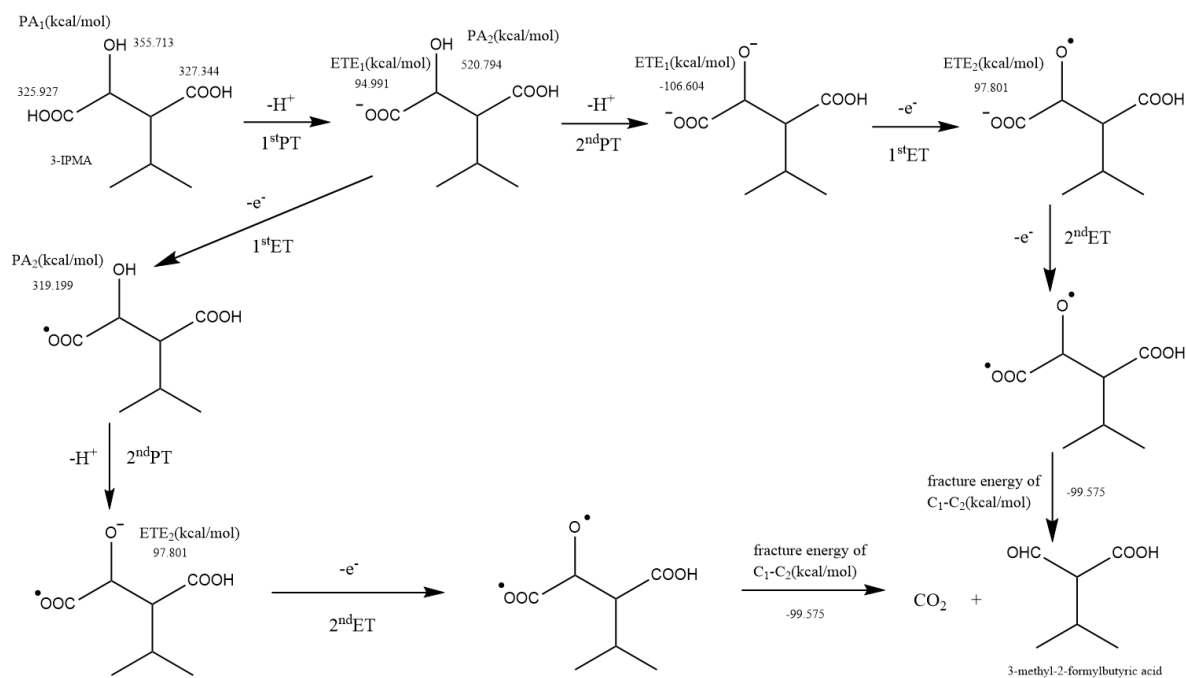**Fig. 8:** SPLET pathway of 2-IPMA in gas-phase. (kcal/mol)

Fig. 9: SPLET pathway of 3-IPMA in gas-phase. (kcal/mol)

Further, the radical scavenging process of 3-IPMA is similar to 2-IPMA, starts with $-C_1OO-$ and ends with the transition of double radical state to singlet state. The total energy cost is 738.343 kcal/moL (Da = PA1+ PA2+ ETE1+ ETE2-FE), similar to 2-IPMA. As expected, the energy required for the SPLET is 738.343 kcal/moL, similar to that of the dianionic pathway.

The dET-PT Mechanism

The required enthalpies for the dET-PT pathway were

calculated in the gas phase, as was done for the SPLET pathway. The ET-PT mechanism, which consists of free radical cations and free radical states, is characterized by the Ionization Potential (IP) and Proton Dissociation Enthalpy (PDE). The enthalpy values for electrons, ions, and free radicals used in this mechanism are presented in Table (S4).

The dET-PT pathway of 2-IPMA, as illustrated in Fig. (10), began with the extraction of an electron from 2-IPMA to form an unstable cationic radical. The active site with the lowest PDE was selected for deprotonation to form a single free radical. Subsequently, the second electron transfer resulted in a cationic intermediate and the structure changed to form a stable singlet product (4-methyl-3-oxopentanoic acid). Further, the total energy cost for this process was 724.270 kcal/moL (IP1+PDE1+IP2+PDE2-FE). The dET-PT pathway of 3-IPMA, depicted in Fig. (11), was found to be similar to that of 2-IPMA, with a total energy cost of 738.343 kcal/mol. It was also evident that the total energy cost was similar when compared with the SPLET pathway.
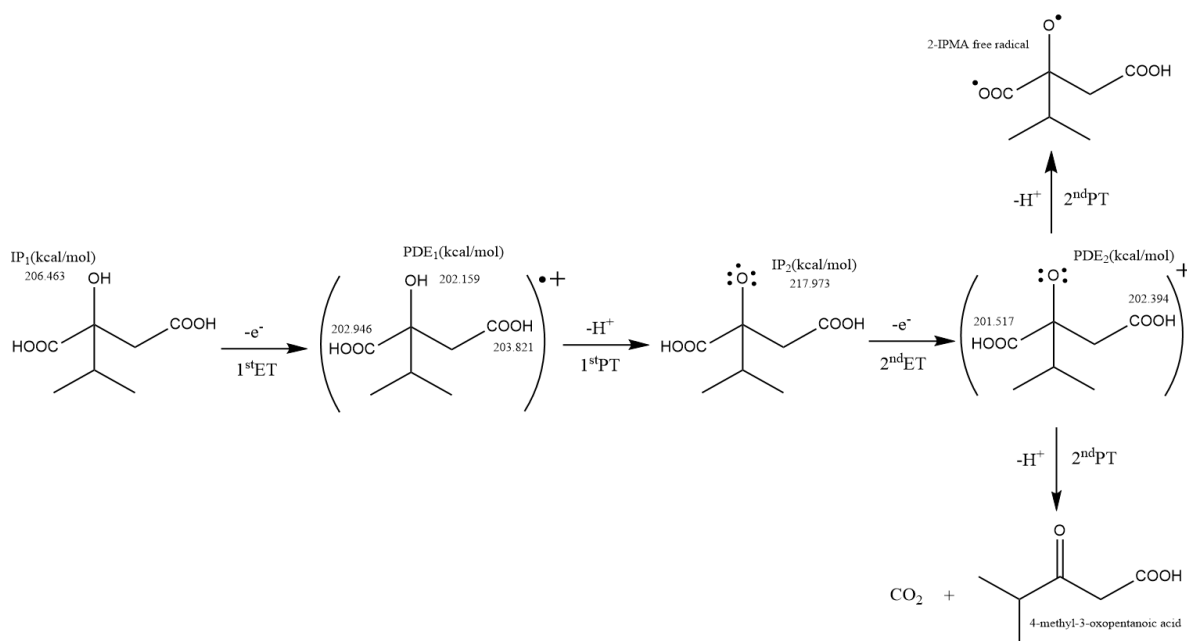

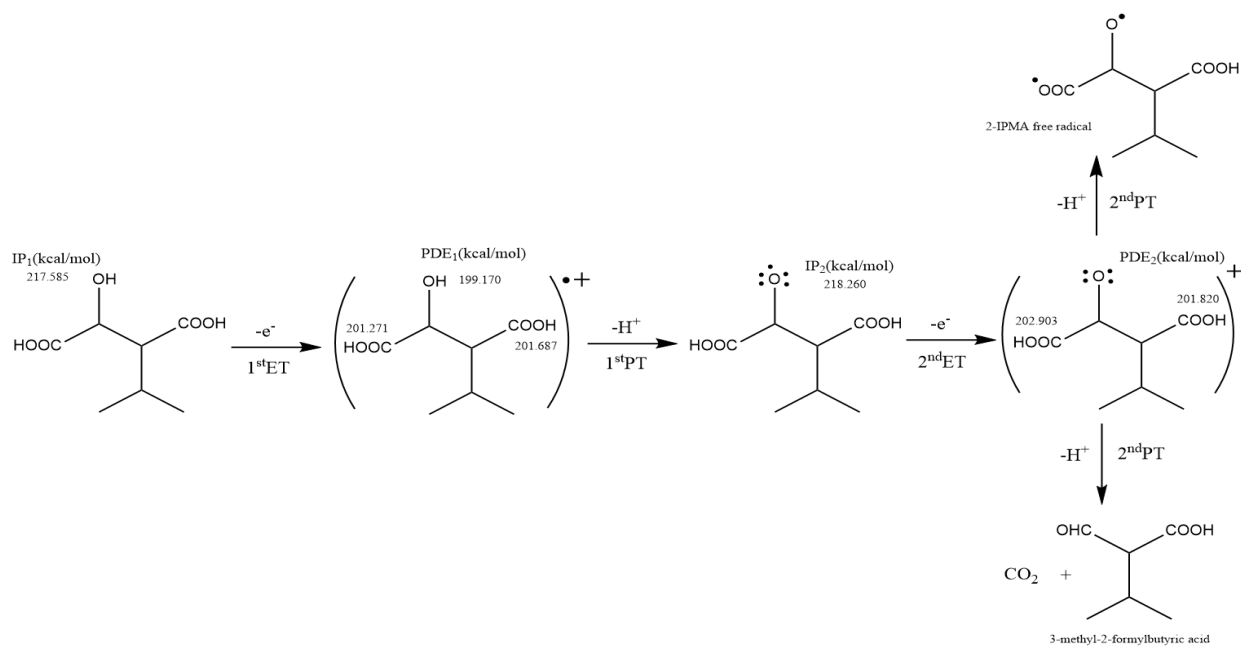**Fig. 10:** dET-PT pathway of 2-IPMA in gas-phase. (kcal/mol)

Fig. 11: dET-PT pathway of 3-IPMA in gas-phase. (kcal/mol)

Cost of Free Radical Scavenging

Exothermic process and low heat absorption are the thermodynamically most likely to occur (Pérez-González *et al.*, 2015) The total energy cost of 2-IPMA and 3-IPMA through HAT, SPLET, and ET-PT pathways is shown in Tables (8-10). Furthermore, the HAT pathway, which occurs in the gas phase, was identified as the lowest-cost pathway for 2-IPMA and 3-IPMA to scavenge free radicals. In addition, the total energy costs for 2-3-IPMA were 101.101-115.926 kcal/moL, respectively,

significantly lower than those of the SPLET and ET-PT pathways.

The SPLET and ET-PT pathways of 2-IPMA and 3-IPMA have the same energy requirements, as shown in Fig. (12), indicating that the two pathways may occur simultaneously (Aljerf and Aljerf, 2023). Furthermore, considering the values of BDE1, PA1, and IP1 and adhering to the principle that the lower cost process tends to occur first, the sequence of antioxidant pathways for 2-IPMA and 3-IPMA is predicted to be HAT, followed by ET-PT and then SPLET.

Table 8: Thermal enthalpies of reaction for HAT mechanisms of radical scavenging by 2-3-IPMA in gas-phase. (in Hartree)

		HAT$_{1st}$				HAT$_{2nd}$				Fracture energy (C$_1$-C$_2$,) (kcal/mol)
		H$_r$	H$_h$	H$_I$	BDE (kcal/mol)	H$_r$	H$_h$	H$_I$	BDE (kcal/mol)	
2-IPMA	C$_1$	-649.533			0.148877 (93.422)	-648.869	-0.5	-649.534	0.164941 (112.308)	0.165483 (-103.842)
	C$_2$	-649.534	-0.5	-650.182	0.147623 (92.635)					
	C$_4$	-649.532			0.150272 (94.297)	-648.868	-0.5	-649.534	0.166340 (113.351)	
3-IPMA	C$_1$	-649.525			0.167218 (102.167)	-649.044	-0.5	-649.532	0.167607 (114.733)	0.158683 (-99.575)
	C$_2$	-649.532	-0.5	-650.192	0.160584 (100.768)					
	C$_4$	-649.528			0.164593 (103.284)	-649.047	-0.5	-649.532	0.165881 (112.89)	

Table 9: Thermal enthalpies of reaction for SPLET mechanisms of radical scavenging by 2-3-IPMA in gas-phase. (kcal/mol)

		Sa-SPLET				Da-SPLET				Fracture energy (C$_1$-C$_2$) (kcal/mol)
		PA$_1$	ETE$_1$	PA$_2$	ETE$_2$	PA$_1$	PA$_2$	ETE$_1$	ETE$_2$	
2-IPMA	C$_1$	315.543	93.867			315.543				
	C$_2$	347.856		324.870	93.832	347.856	528.012	-109.275	93.832	-103.842
	C$_4$	334.821				334.821				
3-IPMA	C$_1$	325.927	94.991			325.927				
	C$_2$	355.713		319.199	97.801	355.713	520.794	-106.604	97.801	-99.575
	C$_4$	327.344				327.344				

Table 10: Thermal enthalpies of reaction for ET-PT mechanisms of radical scavenging by 2-3-IPMA in gas-phase. (kcal/mol)

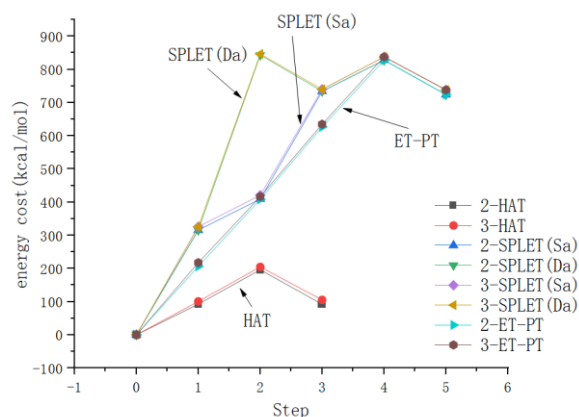|		ET-PT				Fracture energy (C$_1$-C$_2$) (kcal/mol)
		IP$_1$	PDE$_1$	IP$_2$	PDE$_2$	
2-IPMA	C$_1$		202.946		201.517	-103.842
	C$_2$	206.463	202.159	217.973		
	C$_4$		203.821		202.394	
3-IPMA	C$_1$		201.271		202.903	-99.575
	C$_2$	217.585	199.170	218.260		
	C$_4$		201.687		201.820	

Fig. 12: Cumulative energy cost of reaction for three mechanisms of radical scavenging by 2-3-IPMA in gas-phase. (kcal/mol)

Conclusion

2-IPMA and 3-IPMA are organic acids that contain an isopropyl group and belong to the malic acid family. Malic acid and its isomers play important roles in biochemical processes, particularly in relation to energy metabolism and antioxidant defense mechanisms. The study leverages DFT to evaluate the conformations and thermodynamic properties related to their antioxidant activities. Based on thermodynamic calculations, it is inferred that the C2-hydroxy groups of 2-IPMA and 3-IPMA show notable antioxidant activity. The study predicts that 2-IPMA and 3-IPMA would predominantly undergo hydrogen loss through double hydrogen atom transfer (HAT), sequential double proton loss double electron transfer (SPLET), and double electron transfer proton transfer (dET-PT) mechanisms in the gas phase, leading to the formation of specific acid products. The thermodynamic stability of the singlet state over the triplet state in most antioxidants is considered and the pathways for radical scavenging by 2-IPMA and 3-IPMA are theorized to follow the order of HAT, bond dissociation energy (BDE) and SPLET, based on the principle of minimum energy consumption. Calculations confirm the hypotheses, suggesting that the oxidation resistance of the two MA analogs favors the HAT process in terms of reaction enthalpy thermodynamics. The research also meticulously applies thermodynamic data to calculate enthalpy (ΔH) and free energy (ΔG) for reactive species at 298.15 K, a standard temperature in thermodynamics that approximates room temperature.

This research concerning the validation of antioxidant activity and the thermodynamic inference of malic acid and its structural analogs was carried out under *in vitro* conditions, which may fail to accurately mirror the additional factors present in the in vivo environment, such as enzyme activity and cellular metabolism, influencing their antioxidant functions. The computational processes utilized standard states (298.15 K, 1 atm), which may not correspond to physiological conditions, and the actual solvent environment can also affect the thermodynamics of reactions. Thermodynamic inferences do not fully account for the dynamic interactions between antioxidants and other biomolecules, potentially affecting the outcomes. Additionally, the concentration of antioxidants and other reactants, as well as the ionization state of molecules at physiological pH, may influence their antioxidant capabilities, considerations that have not been sufficiently addressed within the thermodynamic models.

Despite the *in vitro* nature of the study, which may not fully encapsulate the in vivo environment's complexity, the findings provide valuable insights into the thermodynamics of antioxidant mechanisms for these compounds. The results are instrumental for understanding the feasibility and spontaneity of the HAT, SPLET, and dET-PT processes in antioxidant activity, offering a foundation for further research into the potential health benefits and applications of these malic acid analogs.

Currently, there is limited research specifically addressing the antioxidant properties of 2-IPMA and 3-IPMA. However, given the importance of antioxidants in maintaining cellular health and preventing chronic diseases, further investigation into the antioxidant potential of these compounds is warranted. Future studies could explore the antioxidant activity of 2-3-IPMA *in vitro* and in vivo, assess their ability to protect cells against oxidative stress, and investigate their potential therapeutic applications in diseases associated with oxidative stress.

Author's Contributions

Han Wu: Conceptualization.
Wenhao Dong: Methodology.
Yanhong Qiu: Writing-original draft preparation.
Changbin Liu: Writing review and editing.

Ethics

This research was exempt from the requirement of ethics committee review or approval because it did not entail the utilization of patient information or the involvement of experimental animals.

References

Aljerf, L., & Aljerf, N. (2023). Food Products Quality and Nutrition in Relation to Public. Balancing Health and Disease: Food Safety and Hygiene Promotion. *Progress in Nutrition*, 25(1), e2023024. https://doi.org/10.23751/pn.v25i1.13928

Amic, A., Lučić, B., Markovic, Z., & Amic, D. (2017). Carboxyl Group as a Radical Scavenging Moiety: Thermodynamics of 2H + /2e – Processes of Phloretic Acid. *Croatica Chemica Acta*, 89(4). https://doi.org/10.5562/cca3024

Amic, A., Zoran, M., Erik, K., Dimitrić Marković, J. M., & Dejan, M. (2018). Theoretical Study of the Thermodynamics of the Mechanisms Underlying Antiradical Activity of Cinnamic Acid Derivatives. *Food Chemistry*, 246, 481–489. https://doi.org/10.1016/j.foodchem.2017.11.100

Annia, G., Gloria, M., Ruslán, A.-D., Tiziana, M., J. Raúl, A.-I., & Nino, R. (2016). Food Antioxidants: Chemical Insights at the Molecular Level. *Annual Review of Food Science and Technology*, 7(1), 335–352. https://doi.org/10.1146/annurev-food-041715-033206

Anouar, E., Kosinova, P., Kozlowski, D., Mokrini, R., Duroux, J. L., & Trouillas, P. (2009). New Aspects of the Antioxidant Properties of Phenolic Acids: A Combined Theoretical and Experimental Approach. *Physical Chemistry Chemical Physics*, 11(35), 7659–7668. https://doi.org/10.1039/B904402G

Ansgar, S., Christian, H., & Reinhart, A. (1994). Fully Optimized Contracted Gaussian Basis Sets of Triple Zeta Valence Quality for Atoms Li to Kr. *The Journal of Chemical Physics*, 100(8), 5829–5835. https://doi.org/10.1063/1.467146

Ansgar, S., Hans W., H., & Reinhart, A. (1992). Fully Optimized Contracted Gaussian Basis Sets for Atoms Li to Kr. *The Journal of Chemical Physics*, 97(4), 2571–2577. https://doi.org/10.1063/1.463096

Aruoma, O. I. (1998). Free Radicals, Oxidative Stress, and Antioxidants in Human Health and Disease. *JAOCS*, 75(2), 199–212. https://doi.org/10.1007/s11746-998-0032-9

Becke, A. D. (1993). Density-Functional Thermochemistry. III. The Role of Exact Exchange. *The Journal of Chemical Physics*, 98(7), 5648–5652. https://doi.org/10.1063/1.464913

Bin, S., Jiancheng, Y., Tianyu, T., Li, Y., & Yanlin, T. (2021). Study on UV Spectrum and Antioxidant Properties of 3-Tert-Butyl-4-Hydroxyanisole Molecule. *Russian Journal of Physical Chemistry A*, 95(2), 343–348. https://doi.org/10.1134/S0036024421020230

Blois, M. S. (1958). Antioxidant Determinations by the Use of a Stable Free Radical. *Nature*, 181(4617), 1199–1200. https://doi.org/10.1038/1811199a0

Borges, R. S., Nagurniak, G. R., Queiroz, L. M. D., Maia, C. S. F., Barros, C. A. L., Orestes, E., & da Silva, A. B. F. (2016). Structure and Toxicity of Clozapine and Olanzapine on Agranulocytosis. *Medicinal Chemistry Research*, 25(2), 322–328. https://doi.org/10.1007/s00044-015-1484-8

Brand-Williams, W., Cuvelier, M. E., & Berset, C. (1995). Use of a Free Radical Method to Evaluate Antioxidant Activity. *LWT - Food Science and Technology*, 28(1), 25–30. https://doi.org/10.1016/S0023-6438(95)80008-5

Burkhard, M., Savin, A., Stoll, H., & Preuss, H. (1989). Results Obtained with the Correlation Energy Density Functionals of Becke and Lee, Yang and Parr. *Chemical Physics Letters*, 157(3), 200–206. https://doi.org/10.1016/0009-2614(89)87234-3

Chengteh, L., Weitao, Y., & Robert G., P. (1988). Development of the Colle-Salvetti Correlation-Energy Formula into a Functional of the Electron Density. *Physical Review B*, 37(2), 785–789. https://doi.org/10.1103/PhysRevB.37.785

Damian, M., Małgorzata, S., Marcin, M., & Rafał, G. (2010). Quantum-Chemical Study on the Antioxidation Mechanisms of Trans-Resveratrol Reactions with Free Radicals in the Gas Phase, Water and Ethanol Environment. *Journal of Molecular Structure: THEOCHEM*, 951(1–3), 37–48.

Dunning, T. H. Jr., Xu, L. T., Cooper, D. L., & Karadakov, P. B. (2021). Spin-Coupled Generalized Valence Bond Theory: New Perspectives on the Electronic Structure of Molecules and Chemical Bonds. *The Journal of Physical Chemistry A*, 125(10), 2021–2050. https://doi.org/10.1021/acs.jpca.0c10472

Eklund, P. C., Långvik, O. K., Wärnå, J. P., Salmi, T. O., Willför, S. M., & Rainer, E. S. (2005). Chemical Studies on Antioxidant Mechanisms and Free Radical Scavenging Properties of Lignans. *Organic and Biomolecular Chemistry*, 3(18), 3336–3347. https://doi.org/10.1039/b506739a

Erik, K., & Vladimír, L. (2006). DFT/B3LYP Study of the Substituent Effect on the Reaction Enthalpies of the Individual Steps of Single Electron Transfer−Proton Transfer and Sequential Proton Loss Electron Transfer Mechanisms of Phenols Antioxidant Action. *The Journal of Physical Chemistry A*, 110(44), 12312–12320. https://doi.org/10.1021/jp063468i

Frankel, E. N., German, J. B., Kinsella, J. E., Parks, E., & Kanner, J. (1993). Inhibition of Oxidation of Human Low-Density Lipoprotein by Phenolic Substances in Red Wine. *The Lancet*, *341*(8843), 454–457. https://doi.org/10.1016/0140-6736(93)90206-V

Frisch, M. J., Trucks, G. W., & Schlegel, H. B. (2016). Gaussian 16, Revision C.01. *Gaussian Inc., Wallingford CT, 1*.

Frankel, E. N., Waterhouse, A. L., & Teissedre, P. L. (1995). Principal Phenolic Phytochemicals in Selected California Wines and Their Antioxidant Activity in Inhibiting Oxidation of Human Low-Density Lipoproteins. *Journal of Agricultural and Food Chemistry*, *43*(4), 890–894. https://doi.org/10.1021/jf00052a008

Ginter, E., Simko, V., & Panakova, V. (2014). Antioxidants in Health and Disease. *Bratisl Lek Listy*, *115*(10), 603–606. https://doi.org/10.4149/bll_2014_116

Guo, H., Wang, N., & Li, X. (2021). Antioxidative Potential of Metformin: Possible Protective Mechanism against generating OH radicals. *Frontiers of Environmental Science & Engineering*, *15*(21), 1–9. https://doi.org/10.1007/s11783-020-1313-2

Halliwell, B., Gutteridge, J. M. C., & Cross, C. E. (1992). Free Radicals, Antioxidants, and Human Disease: Where are We Now? *The Journal of Laboratory and Clinical Medicine*, *119*(6), 598–620.

Humphrey, W., Dalke, A., & Schulten, K. (1996). VMD: Visual Molecular Dynamics. *Journal of Molecular Graphics*, *14*(1), 33–38. https://doi.org/10.1016/0263-7855(96)00018-5

Hussain, S. P., Hofseth, L. J., & Harris, C. C. (2003). Radical Causes of Cancer. *Nature Reviews. Cancer*, *3*(4), 276–285. https://doi.org/10.1038/nrc1046

Junxing, Z., Qian, L., Ruixin, Z., Wenzhong, L., Youshe, R., Chunxiang, Z., & Jianxin, Z. (2018). Effect of dietary grape pomace on growth performance, meat quality and antioxidant activity in ram lambs. *Animal Feed Science and Technology*, *236*, 76–85. https://doi.org/10.1016/j.anifeedsci.2017.12.004

Junxing, Z., Yaqian, J., Min, D., Liu, W., Ren, Y., Zhang, C., & Zhang, J. (2017). The Effect of Dietary Grape Pomace Supplementation on Epididymal Sperm Quality and Testicular Antioxidant Ability in Ram Lambs. *Theriogenology*, *97*, 50–56. https://doi.org/10.1016/j.theriogenology.2017.04.010

Jiang, X., Tao, L., Li, C., You, M., Li, G. Q., Zhang, C., & Hu, F. (2020). Grouping, Spectrum–Effect Relationship and Antioxidant Compounds of Chinese Propolis from Different Regions Using Multivariate Analyses and Off-Line Anti-DPPH Assay. *Molecules*, *25*(14), 3243. https://doi.org/10.3390/molecules25143243

Kumaran, A., & Joel karunakaran, R. (2006). Antioxidant and Free Radical Scavenging Activity of an Aqueous Extract of Coleus Aromaticus. *Food Chemistry*, *97*(1), 109–114. https://doi.org/10.1016/j.foodchem.2005.03.032

Karaman, S., Karasu, S., Tornuk, F., Toker, O. S., Gecgel, Ü., Sagdic, O., Ozcan, N., & Gül, O. (2015). Recovery Potential of Cold Press Byproducts Obtained from the Edible Oil Industry: Physicochemical, Bioactive, and Antimicrobial Properties. *Journal of Agricultural and Food Chemistry*, *63*(8), 2305–2313. https://doi.org/10.1021/jf504390t

Lu, T., & Chen, F. (2012). Multiwfn: A Multifunctional Wavefunction Analyzer. *The Journal of Computational Chemistry*, *33*(5), 580–592. https://doi.org/10.1002/jcc.22885

Lu, Y., Wang, A., Shi, P., & Li, Z. (2015). Quantum Chemical Study on the Antioxidation Mechanism of Piceatannol and Isorhapontigenin toward Hydroxyl and Hydroperoxyl Radicals. *PLOS ONE*, *10*(7), e0133259. https://doi.org/10.1371/journal.pone.0133259

Markovic, Z., Dorovic, J., Dimitric Markovic, J. M., Biocanin, R., & Amic, D. (2016). Comparative Density Functional Study of Antioxidative Activity of the Hydroxybenzoic Acids and Their Anions. *Turkish Journal of Chemistry*, *40*(3), 499–509. https://doi.org/10.3906/kim-1503-89

Massimo, R., Simone, M., Roberta, G., Gianni, S., Michele, M., Simone, L., Sauro, V., & Giovanni, C. (2019). Identification and Quantification of New Isomers of Isopropyl-Malic Acid in Wine by LC-IT and LC-Q-Orbitrap. *Food Chemistry*, *294*, 390–396. https://doi.org/10.1016/j.foodchem.2019.05.068

McCord, J. M., & Fridovich, I. (1969). Superoxide Dismutase. An Enzymic Function for Erythrocuprein (Hemocuprein). *The Journal of Biological Chemistry*, *244*(22), 6049–6055.

Natacha, R., Raphaëlle, S., Brigitte, T., Jérémie, C., Elisabeth, V. H., & Jean-Louis, L. (2015). Optimization of Oil Yield and Oil Total Phenolic Dontent During Grape Seed Cold Screw Pressing. *Industrial Crops and Products*, *63*, 26–33. https://doi.org/10.1016/j.indcrop.2014.10.001

Oliveira, C. M., Silva Ferreira, A. C., Victor, D. F., & Artur, M. S. S. (2011). Oxidation Mechanisms Occurring in Wines. *Food Research International*, *44*(5), 1115–1126. https://doi.org/10.1016/j.foodres.2011.03.050

Pérez-Gálvez, A., Isabel, V., Itziar, B., & María, R. (2020). HPLC-hrTOF-MS study of copper chlorophylls: Composition of Food Colorants and Biochemistry after Ingestion. *Food Chemistry*, *321*, 126721. https://doi.org/10.1016/j.foodchem.2020.126721

Pace-Asciak, C. R., Hahn, S., Diamandis, E. P., Soleas, G., & Goldberg, D. M. (1995). The Red Wine Phenolics Trans-Resveratrol and Quercetin Block Human Platelet Aggregation and Eicosanoid Synthesis: Implications for Protection Against Coronary Heart Disease. *Clinica Chimica Acta; International Journal of Clinical Chemistry*, 235(2), 207–219. https://doi.org/10.1016/0009-8981(95)06045-1

Pérez-González, A., Alvarez-Idaboy, J. R., & Galano, A. (2015). Free-Radical Scavenging by Tryptophan and its Metabolites Through Electron Transfer Based Processes. *Journal of Molecular Modeling*, 21(8), 213. https://doi.org/10.1007/s00894-015-2758-2

Pier-Giorgio, P. (2000). Flavonoids as Antioxidants. *Journal of Natural Products*, 63(7), 1035–1042. https://doi.org/10.1021/np9904509

Qiu, S.-S., Jiang, C.-C., Huang, Y., & Zhou, R.-J. (2017). Theoretical Investigation on the Relationship between the Structures and Antioxidant Activities of Myricetin and Dihydromyricetin. *Chinese Journal of Structural Chemistry*, 36(3), 416–422.

Re, R., Pellegrini, N., Proteggente, A., Pannala, A., Yang, M., & Rice-Evans, C. (1999). Antioxidant Activity Applying an Improved ABTS Radical Cation Decolorization Assay. *Free Radical Biology and Medicine*, 26(9–10), 1231–1237. https://doi.org/10.1016/s0891-5849(98)00315-3

Rivera, E. S., Djambazova, K. V., Neumann, E. K., Caprioli, R. M., & Spraggins, J. M. (2020). Integrating Ion Mobility and Imaging Mass Spectrometry for Comprehensive Analysis of Biological Tissues: A Brief Review and Perspective. *Journal of Mass Spectrometry*, 55(12), e4421. https://doi.org/10.1002/jms.4421

Rohan, S., Aditi, K., Kaushik, B., & Supradip, S. (2018). Anthocyanin Composition and Potential Bioactivity of Karonda (Carissa Carandas L.) Fruit: An Indian Source of Biocolorant. *LWT*, 93, 673–678. https://doi.org/10.1016/j.lwt.2018.04.012

Sason, S., David, D., & Philippe C., H. (2021). Valence Bond Theory—Its Birth, Struggles with Molecular Orbital Theory, Its Present State and Future Prospects. *Molecules*, 26(6), 1624. https://doi.org/10.3390/molecules26061624

Shimada, K., Fujikawa, K., Yahara, K., & Nakamura, T. (1992). Antioxidative Properties of Xanthan on the Autoxidation of Soybean Oil in Cyclodextrin Emulsion. *Journal of Agricultural and Food Chemistry*, 40, 945–948. https://doi.org/10.1021/jf00018a005

Stéphanie, D., Xavier, V., Philippe, C., Marion, W., & Jean-Michel, M. (2009). Comparative Study of Antioxidant Properties and Total Phenolic Content of 30 Plant Extracts of Industrial Interest Using DPPH, ABTS, FRAP, SOD, and ORAC Assays. *Journal of Agricultural and Food Chemistry*, 57(5), 1768–1774. https://doi.org/10.1021/jf803011r

Tian, L., & Fei-Wu, C. (2011). Calculation of Molecular Orbital Composition. *Acta Chimica Sinica*, 69(20), 2393–2406.

Wootton-Beard, P. C., Aisling, M., & Lisa, R. (2011). Stability of the Total Antioxidant Capacity and Total Polyphenol Content of 23 Commercially Available Vegetable Juices Before and After *in vitro* Digestion Measured by FRAP, DPPH, ABTS and Folin–Ciocalteu Methods. *Food Research International*, 44(1), 217–224. https://doi.org/10.1016/j.foodres.2010.10.033

Xican, L. (2017). 2-Phenyl-4,4,5,5-Tetramethylimidazoline-1-Oxyl 3-Oxide (PTIO•) Radical Scavenging: A New and Simple Antioxidant Assay *in vitro*. *Journal of Agricultural and Food Chemistry*, 65(30), 6288–6297. https://doi.org/10.1021/acs.jafc.7b02247

Xican, L. (2018). Comparative Study of 1,1-Diphenyl-2-Picryl-Hydrazyl Radical (DPPH•) Scavenging Capacity of the Antioxidant Xanthones Family. *ChemistrySelect*, 3(46), 13081–13086. https://doi.org/10.1002/slct.201803362

Xilan, T., Jian-Xun, L., Wei, D., & Peng, L. (2013). Evid-Based. *Evidence-Based Complementary and Alternative Medicine: ECAM*, 2013(3), 820695. https://doi.org/10.1155/2013/820695

Yunus, K., Yilmaz, V. T., & Buyukgungor, O. (2016). Synthesis, Spectroscopic, Structural and Quantum Chemical Studies of a New Imine Oxime and Its Palladium(II) Complex: Hydrolysis Mechanism. *Molecules*, 21(1), 52. https://doi.org/10.3390/molecules21010052

Zhongping, T., Qingwei, K., Yi, L., Weiguo, X., Jingping, Q., Hua, C., & Xisheng, F. (2014). Theoretical Studies on the Structure and Property of Alkylated Dipenylamine Antioxidants. *Journal of Theoretical and Computational Chemistry*, 13(5), 1450035. https://doi.org/10.1142/S0219633614500357